Nanomedicine

Fluorescein-entrapped magnetosomes for magnetically assisted photodynamic therapy

Journal:	*Nanomedicine*
Manuscript ID	NNM-2020-0445.R1
Manuscript Type:	Conference Report
Keywords:	Magnetosomes, Fluorescein, Photodynamic therapy, Magnetic targeting, in vitro cytotoxicity

Future Medicine

Version: 19th June 2020

Article Body Template

Abstract:

Aims: We investigated the application of fluorescein (FL) entrapped magnetosomes, i.e. silica-coated iron oxide nanoparticles entrapped within niosomes (SIO/NIO), in magnetically assisted photodynamic therapy (PDT) *in vitro*. **Materials and Methods:** Panc-1 cells were treated with the magnetosomes, with and without external magnetic guidance, and irradiated with blue light. **Results and Conclusions:** Upon photoactivation, the FL-entrapped magnetosomes can produce higher singlet oxygen in comparison to FL-entrapped micelles, probably due to the higher release tendency of the photosensitizer from the former. *In vitro* studies in Panc-1 cells revealed magnetically assisted enhancement in the cellular uptake of the magnetosomes. Magnetic assistance also led to enhancement in PDT efficiency in cells treated with the FL-entrapped magnetosomes and light, thus highlighting their potential in PDT.

Graphical Abstract:

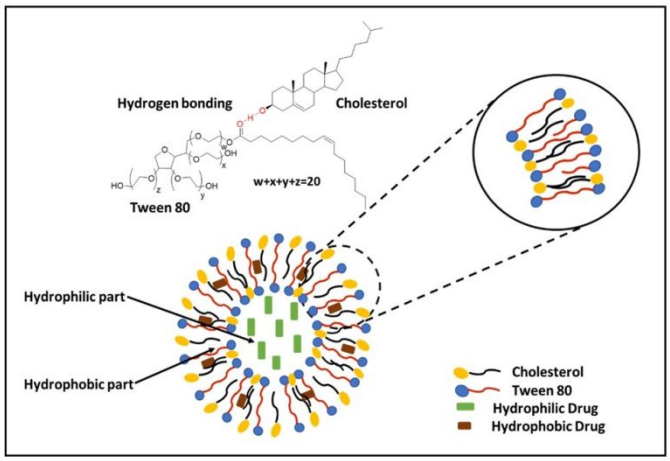

Mechanism of drug encapsulation within niosomal nanocarriers

Keywords: Magnetosomes; Fluorescein; Photodynamic therapy; Magnetic targeting; in vitro cytotoxicity.

Future Medicine
Version: 19th June 2020

Article Body Template

Introduction:

Bilayered vesicular drug delivery systems are known to entrap both hydrophilic and lipophilic drugs in their interior compartments and enhance their bioavailability [1-7]. They can also incorporate small sized nanoparticles, thus reducing their agglomeration and enhancing their biocompatibility and circulation time [8,9]. Niosomes (NIO) are a class of vesicular nanocarriers which are composed of non-ionic surfactants (e.g. Triton X-100, alkyl ether) and cholesterol [10-12]. The major advantages of niosomes include rendering enhanced solubility of poorly water soluble drugs and smaller nanoparticles [13], along with improved stability and bioavailability of entrapped agents [14,15]. They are known to enhance the anticancer activity of loaded drugs *via* precision delivery and controlled release at the site of action [16-18]. For example, photosensitizer loaded niosomes have been used to enhance the transdermal delivery of photosensitizers for effective photodynamic therapy of skin cancer [19,20].

Iron oxide-based nanoparticles are widely used for several biomedical applications, such as magnetically-assisted drug targeting, MRI contrast enhancement, magnetic hyperthermia therapy (MHT), and simulation-guided photothermal therapy [21-30]. Owing to their ultrasmall size, they can be incorporated within larger vesicular nanocarriers, thus imparting magnetic properties in these carriers. Such 'magnetosomes' can be co-incorporated/entrapped with additional active agents, such as anticancer drugs, for use in magnetically-targeted, image-guided therapies and theranostics. In this work, we report the preparation of magnetosomes composed of silica-coated iron-oxide (SIO) nanoparticles entrapped within niosomes. These SIO/NIO magnetosomes are further entrapped with the dye/photosensitizer fluorescein (FL), which is known to convert molecular oxygen ($^3O_2$) into cytotoxic singlet oxygen ($^1O_2$) upon irradiation with blue laser/LED light. FL is a well-known photosensitizer in photodynamic therapy (PDT), with potential applications in treating cancer, pathogenic infections, and some other diseases [31-33]. Therefore, the entrapment of FL within SIO/NIO magnetosomes is expected to provide magnetically assisted PDT in cancer and other diseased cells.

The magnetosomes were characterized using common techniques, such as TEM and DLS to examine their morphology, EDS to determine their elemental composition, FTIR to confirm the

Future Medicine

Version: 19th June 2020

various coatings, and VSM to know their magnetic properties. Optical properties of FL-SIO/NIO magnetosomes were examined by UV-visible and fluorescence spectroscopic techniques. Finally, they were analyzed for their *in vitro* activity by examining their magnetically induced cellular uptake and PDT efficacy in Panc-1 cancer cells.

Materials & Methods:

Synthesis of silica-coated iron oxide (SIO) nanoparticles:

Synthesis of IO nanoparticles were carried out by co-precipitation method [34]. In detail, 0.473g (0.146 M) $FeCl_3$ and 0.198 g of $FeCl_2$ (0.078M) were added in 20 mL of double distilled water (DDW). The solution was stirred for half an hour at 80°C under N_2 atmosphere to obtain a homogeneous mixture. After that, 2.5 mL aqueous ammonia solution was added to the system. N_2 atmosphere was maintained for another half hour. The synthesized IO nanoparticles were washed with DDW and separated with the help of a rare-earth bar magnet (5 cm x 5 cm).

For silica coating, IO nanoparticles were dispersed in 1:4 water/ethanol system. To this system, 10µl the silica precursor vinyltriethoxysilane (VTES) was added, which is hydrolysed by the addition of glacial acetic acid. The solution was kept for overnight stirring at 25°C. The resulting SIO nanoparticles were washed with water:ethanol mixture and collected with the help of the bar magnet [35]. They were finally dispersed in DMSO prior to entrapment within niosomes.

Preparation of SIO/NIO magnetosomes and co-entrapment of FL:

The non-ionic surfactant (Tween-80, 0.2g) and the lipid cholesterol (0.2g) were mixed in an organic solvent (diethyl ether, 2 ml) and stirred to get a homogeneous solution. After that, 1 ml of this solution was added dropwise to pre-heated DDW (10 ml). For preparing FL and SIO co-entrapped niosome, 100µl of FL in DMSO (15 mM) and 100µl of SIO in DMSO (9mg/ml) were also added to this system. The solution was slowly stirred for 30 mins at 70°C, followed by separation with the help of a bar magnet. The obtained SIO/NIO nanoparticles were further purified by dispersing in DDW and separated again with the help of the external magnet. This procedure was repeated three times. After dispersing the separated product in DDW, it was further purified by centrifugation (15,000 rpm for 10 minutes at room temperature) and washing

in DDW, and then kept aside for further use. The synthesis of fluorescein (FL) and SIO nanoparticle co-entrapped niosomes (FL-SIO/NIO) is shown schematically in Figure 1. A control (FL-Micelles) was also prepared by dropwise addition of equivalent amount of FL (100µl of 15 mM FL in DMSO) in 11 ml of tween-80 micelles.

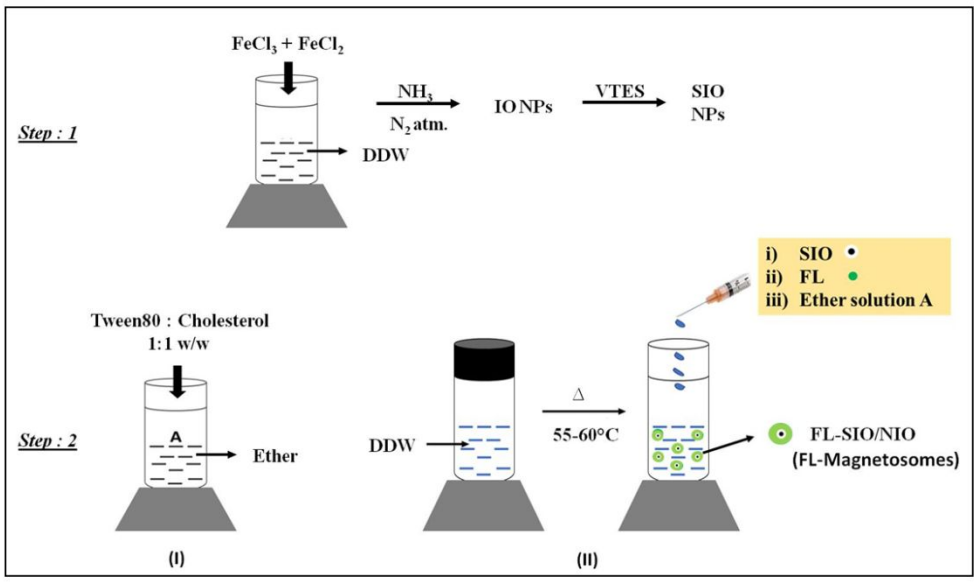

Figure 1: Schematic representation for the synthesis of fluorescein (FL) and SIO nanoparticle co-entrapped niosomes (FL-SIO/NIO).

Characterization studies:

Fourier transform infrared (FTIR) spectra was recorded with the help of Perkin Elmer RX1 spectrometer by mixing 3 mg of the dried niosomes with KBR powder. This mixture was then pressed by hydraulic pressure machine to form a pallet, which was then analyzed to record the spectra in the range of 4000 to 400 cm^{-1}.The magnetic properties of the niosomes were examined *via* vibrating sample magnetometry (VSM) with the help of 3473-70 electromagnet amplifier (CREST Performance CPX 900 power amplifier machine). For this, 2mg of the niosomes were wrapped in a Teflon tape and placed inside the VSM machine to measure the magnetization.

Future Medicine

Version: 19th June 2020

Article Body Template

The hydrodynamic sizes of the IO nanoparticles and SIO/NIO magnetosomes were calculated by dynamic light scattering (DLS) measurements. Herein, diluted aqueous dispersion of the samples were poured into a glass cuvette and analyzed using a NANO-ZS series MALVERN ZETASIZER. The samples were also analyzed by transmission electron microscope (TEM). Herein, the aqueous dispersion of the samples was drop coated and dried on a copper grid (Ted Pella USA), and then examined by TECNAI G2-30 U TWIN TEM instrument. Before drying of the film, it was negatively stained by using 2% aqueous dispersion of phosphotungstic acid. Selected area electron diffraction (SAED) analysis for crystalline diffraction pattern, and energy dispersive spectroscopy (EDAX) for elemental analysis were also carried out using the same instrument.

UV-Visible and fluorescence spectra were recorded to examine the optical properties of the samples. UV-Visible spectra of FL-Micelles, blank NIO and FL-SIO/NIO were recorded by using Shimadzu UV-1601 spectrophotometer. Fluorescence spectra were recorded using Cary Eclipse fluorescence spectrophotometer (Varian, Palo Alto, CA).

Study of drug release and activity

To study the release pattern of entrapped FL from magnetosomes, niosomes and tween-80 micelles, 2 mL aqueous dispersion of the FL-SIO/NIO, FL-NIO and FL-Micelles were taken in a dialysis bag and suspended against DDW for a period of 5 days. Because of the low cut-off pore size (14 KD) of the dialysis bag, only free FL can diffuse out of the membrane into the bulk water. We have examined the percentage of the FL released per day by measuring the optical density of the bulk water using fluorescence spectrophotometer at λ_{exc} = 480 nm.

ABMDMA [9,10-anthracenediyl-bis(methylene)dimalonic acid] bleaching assay was used for the detection of singlet oxygen generation following photo-irradiation of FL, by observing the decay in absorption at 380nm *via* UV-Visible spectroscopy. In a typical experiment, 20µL of the sodium salt of ABMDMA (15 µM) was mixed separately with various samples (FL-SIO/NIO, FL-NIO and FL-Micelles) dispersed in water, having the final normalized concentration of 2.5µM for FL in each case. The solutions were irradiated for 0, 5 and 10 mins in a 3 ml vial

using blue light (50 mW/cm^2). Then, the optical densities at 380 nm were recorded in the UV-Vis spectrometer as a function of irradiation time.

In vitro studies

The cellular uptake study of FL-Micelles and FL-SIO/NIO was carried out by fluorescence microscopy of treated cells, as well as fluorometric analysis of treated and lysed cells. Fluorescence microscopy was done by treating two sets of 35 mM cell plates, containing Panc-1 cells seeded overnight at ~ 60% confluence, with FL-Micelles and FL-SIO/NIO (each with 3.0 µM of FL). Cells treated with equivalent amount of placebo (non FL-loaded) SIO/NIO magnetosomes (0.5 mg/ml) were used as controls. External magnetic field was applied by placing the rare earth bar magnet (5 cm x 5 cm) below the one set of plates for 10 mins, while the other set did not receive any external magnetic guidance. After incubating all the plates for two hours, they were washed with PBS and observed directly under a Nikon Eclipse Ti2 inverted microscope for imaging.

In addition to this, the cellular uptake was also analysed by fluorometric analysis of lysates of treated cells. Here also, two sets of 35 mM cell plates containing seeded Panc-1 cells were treated with the same samples at the similar concentrations, as discussed above. External magnetic field was applied to only one set of the treated cells, as discussed before. After incubating for two hours, all the plates were washed with PBS and treated with 1% Triton-X 100 (lysis solution). The lysates were scraped, homogenized, and centrifuged to separate the cellular debris. The fluorescence recovered from the cellular lysates were examined by measuring the fluorescence intensity of FL (λ_{ex} = 490 nm and λ_{em} = 540 nm), which semi-quantitatively correlates with the FL uptake in the cells.

The cell viability (MTT) assay was carried out after treating 35 mm plates, containing Panc-1 cells seeded overnight (confluence ~ 60%), with FL-Micelles and FL-SIO/NIO, in the presence and absence of external magnetic force. The final concentration of FL in each well was taken as 3µM of FL in 150 µg/ml of FL-SIO/NIO and 3µM of FL-Micelles. External magnetic force was applied for 10 mins to half of the plates by placing a rare-earth bar magnet (5 cm x 5cm)

Future Medicine

Version: 19th June 2020

underneath them. All the treated plates were then incubated for 2 hrs, washed with PBS, replenished with fresh media, and incubated again. Then, one set of the plates were irradiated for 10 mins with blue light (50 mW/cm^2) and returned to the incubator. After 48 hrs of incubation, cell viability was measured by adding 100µL of MTT reagent (5 mg/mL in FBS) to each plate and further incubation for 2 hours. Then, the media was aspirated and 1mL of DMSO was added in each well to dissolve the formazan crystals. The optical density was measured at 570 nm spectrometrically and the percentage cell viability calculated by arbitrarily assigning the viability of untreated cells as 100%.

Results:

FTIR spectral data was studied to examine the effect of various coatings over the surface of IO NPs. In Figure:2(a), the band appearing at 580 cm^{-1} represents the stretching vibration of Fe-O bonds in IO NPs. The appearance of the absorption bands at around 1083 and 796 cm^{-1} in SIO and SIO/NIO are probably due to the stretching vibrations of Si-O-Si group. The suppression of the peak at 580 cm^{-1} (Fe-O) represents the silica coating over the surface of IO NPs. In addition to this, further suppression in the characteristic peaks of SIO nanoparticles confirms the entrapment of SIO within the vesicular system.

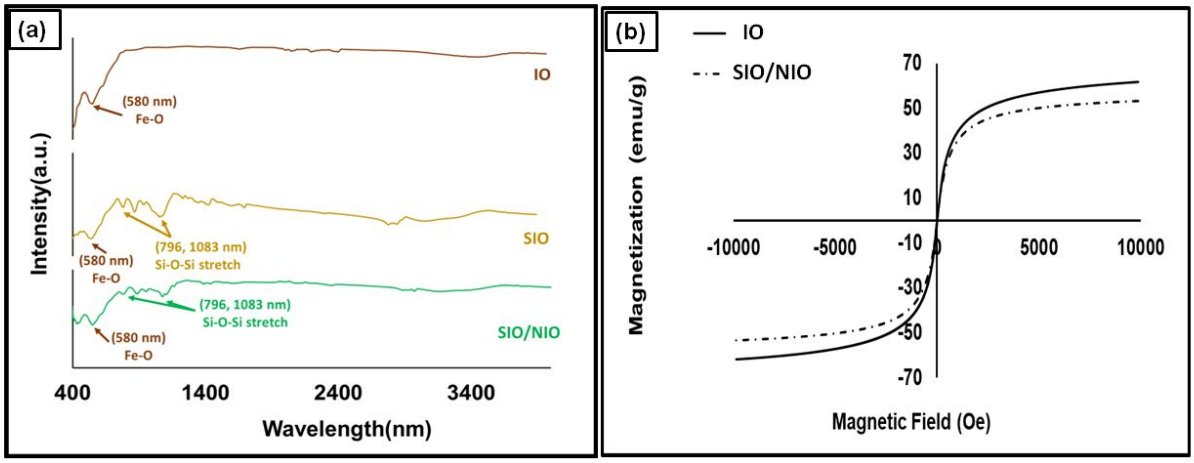

Figure 2:(a) FTIR spectra of iron oxide (IO), silica coated iron oxide (SIO), and SIO entrapped within niosomes (SIO/NIO), or magnetosomes. (b)Magnetization curve showing superparamagnetic nature of IO and SIO/NIO.

Future Medicine
Version: 19th June 2020

Article Body Template

VSM method was used at room temperature to determine the magnetic properties of IO and SIO/NIO, as shown in Figure:2 (b). The saturation magnetization (Ms) obtained from the magnetization curve were found to be around 61.8 and 53.3 emu/g, respectively, for IO nanoparticles and SIO/NIO magnetosomes. This slight decrease in the value of saturation magnetization in SIO/NIO is possibly because of the existence of a magnetically unresponsive silica and niosomal layers over the IO nanocore [36].

TEM analysis was carried out to obtain the size and morphology of the iron oxide (IO) nanoparticles and SIO/NIO magnetosomes, as shown in Figure:3(a,b). The average size of the IO nanoparticles was found to be around 8 nm (Figure:3a), whereas 30-50 nm spherical structure was observed in case of the prepared SIO/NIO magnetosomes (Figure:3b). The presence of few (3-5) SIO nanoparticles are observed within single magnetosomes. The polydispersity of these magnetosomes can be reduced in future with more precision synthesis. The hydrodynamic diameter of the samples was calculated using dynamic light scattering (DLS) technique (Figure:3, c,d). The average size was found to be around 14 nm and 75 nm, for IO (Figure:3c) and SIO/NIO (Figure:3d), respectively, with more polydispersity in the later. The size obtained for these samples using DLS were found to be in agreement with the size calculated by TEM analysis; the slight enhancement in the size observed in the hydrodynamic diameter as measured by DLS is attributed to the hydration layer covering the samples.

Future Medicine

Version: 19th June 2020

Article Body Template

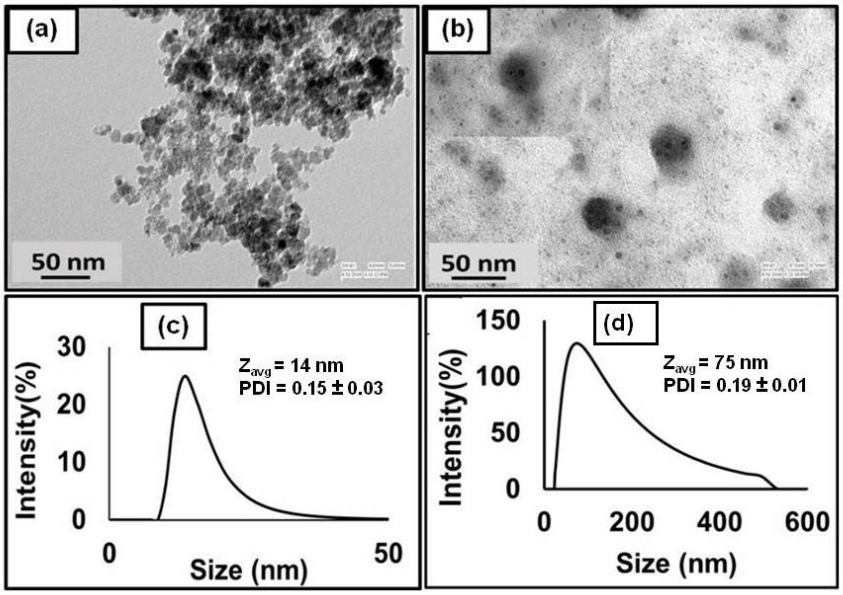

Figure 3: TEM images (a), (b), and DLS graphs (c), (d) of iron oxide (IO) nanoparticles and SIO/NIO magnetosomes.

(Figure:4 a,b) represents the EDAX spectra of the IO nanoparticles and SIO/NIO magnetosomes, determining the elemental composition in the given sample. The spectra shows the presence of Fe, O in case IO (Figure:4a), and Fe, O, Si, C, O in case of SIO/NIO (Figure:4b). The additional elements observed in the SIO/NIO magnetosomes are due to the silica and niosomal coatings on the iron oxide nanocores.

Future Medicine
Version: 19th June 2020

Article Body Template

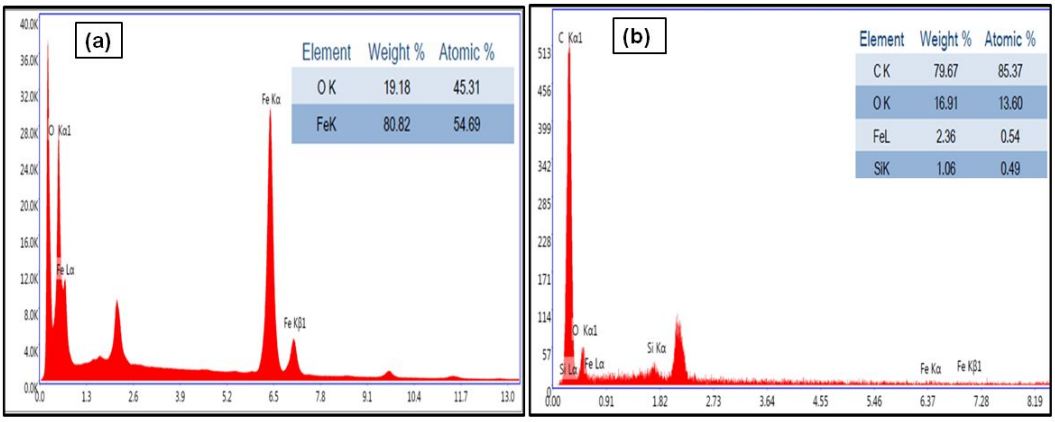

Figure 4: EDAX spectra of (a) Iron oxide (IO) nanoparticles and (b) SIO/NIO magnetosomes.

Figure:5a represents the UV-visible absorption spectrum of FL entrapped tween-80 micelles (FL-Micelles) with the appearance of the characteristic absorption peak of fluorescein at 490 nm. The loading of FL in FL-SIO/NIO magnetosomes was observed by comparing the emission spectra (peak at 520 nm) of FL-Micelles and FL-SIO/NIO magnetosomes (Figure 5b), which were recorded at an excitation wavelength of 490 nm. The data shows that the emission peak of FL is retained when it is entrapped within the magnetosomes, albeit with lower intensity as compared to that of FL-Micelles of normalized optical density. This partial signal attenuation of FL entrapped within magnetosomes is probably due to its entrapped condition, and/or the proximity to iron oxide nanoparticles (a known emission quencher). Nevertheless, the data shows that FL is indeed entrapped within the magnetosomes and retains its emission pattern.

Release studies of FL from FL-SIO/NIO magnetosomes, along with that from FL-NIO niosomes and FL entrapped within tween 80 micelles (FL-Micelles),were examined at 37°C (Figure: 5c). An almost similar sustained release pattern, with about 75-80 percent release of FL within span

Future Medicine

Version: 19th June 2020

Article Body Template

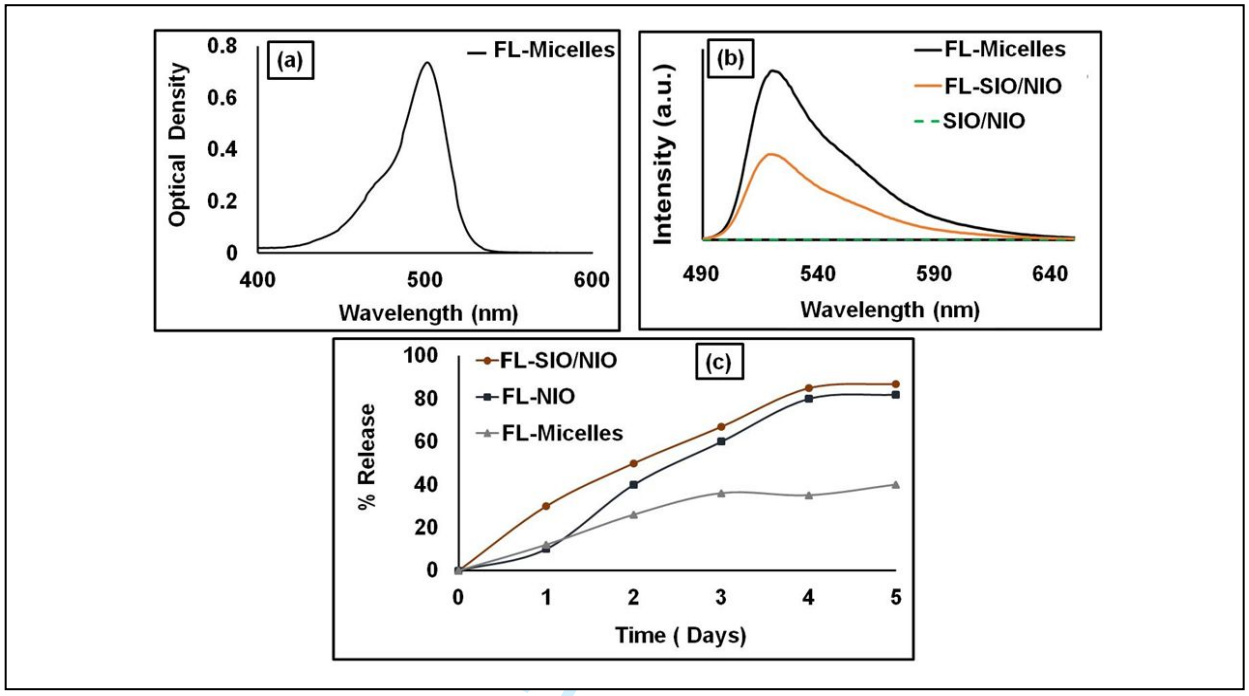

Figure 5:(a)UV-Vis spectra of FL-Micelles, (b) Emission spectra of FL-Micelles, FL-SIO/NIO magnetosomes, and SIO/NIO magnetosomes. (c) Percent Release (%) of fluorescein from FL-NIO niosomes, FL-SIO/NIO magnetosomes, and FL-entrapped tween-80 micelles.

of 5 days, was observed for both FL-entrapped niosomes (FL-NIO) and magnetosomes (FL-SIO/NIO), while only 40 % FL was released from the tween 80 micelles. This shows the FL has a better release pattern from the niosomal/magnetosomal carriers as compared to that of micellar carriers, probably due to that bilayered structure of the niosomes/magnetosomes. It is interesting to note that none of the systems displayed burst release of FL. Overall, it can be concluded that these magnetosomes can be efficiently used in sustained drug delivery, which correlates with our earlier report about the use of magnetically-doped niosomes for sustained release drug delivery.

Detection of singlet oxygen ($^1O_2$) following photoirradiation of FL, in both free and entrapped states, was carried out using ABMDMA as a singlet oxygen ($^1O_2$) detector. ABMDMA is bleached (observed by the reduction in its characteristic absorption peak at 380 nm) upon interaction with singlet oxygen ($^1O_2$) *via* cycloaddition reaction of $^1O_2$ with the anthracene ring of ABMDMA. A graph was plotted between natural log of (A_t/A_0) versus time (min), as shown in Figure 6. The values of rate constant were calculated using the following equation: ln

Future Medicine
Version: 19th June 2020

$([A_t]/[A_0]) = -kt$, where, $[A_0]$ and $[A_t]$ are the optical densities of ABMDMA before and after blue light irradiation, respectively, 'k' is the first order rate constant for the quenching of ABMDMA by $^1O_2$, and 't' is the time of LED light irradiation. From the data (Figure 6), we observed that the singlet oxygen photogeneration efficiency of FL is higher when it is entrapped within niosomes ($k = 0.0462\ min^{-1}$) as well as magnetosomes ($k = 0.0582\ min^{-1}$), in comparison to FL entrapped in tween-80 micelles ($k = 0.025\ min^{-1}$) of the same concentration. This is probably because of the higher release tendency of the photosensitizer from the niosomes and magnetosomes as compared to that from the micelles. Overall, it can be concluded that the photosensitizer activity of FL is not only retained, but also significantly enhanced, when it is entrapped within the magnetosomes.

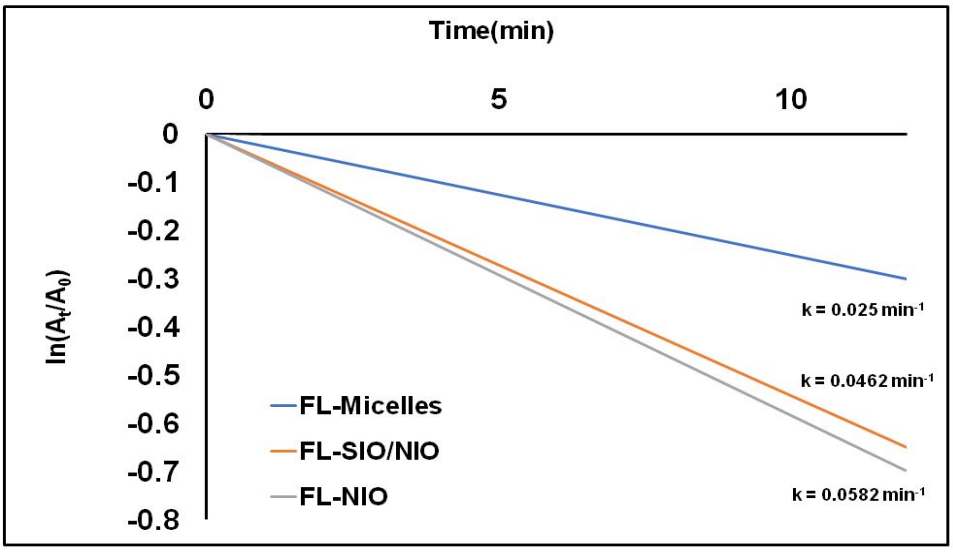

Figure 6: A plot between ln (A_t/ A_0) versus time(min) by measuring optical density of ABMDMA as a function of time of light irradiation

Finally, Panc-1 cells (of human pancreatic cancer origin) were treated with these samples in order to examine their cellular uptake, biocompatibility and PDT efficacy. The cellular uptake of the samples was first probed by using fluorescence microscopy of treated cells. The phase contrast and corresponding fluorescence images of the cells, treated with FL entrapped both in

Future Medicine

Version: 19th June 2020

tween-80 micelles (FL-micelles) and in magnetosomes (FL-SIO/NIO), with and without external magnetic force, is depicted in Figure 7. The phase contrast images (Figure 7: a, b, e, f) show that

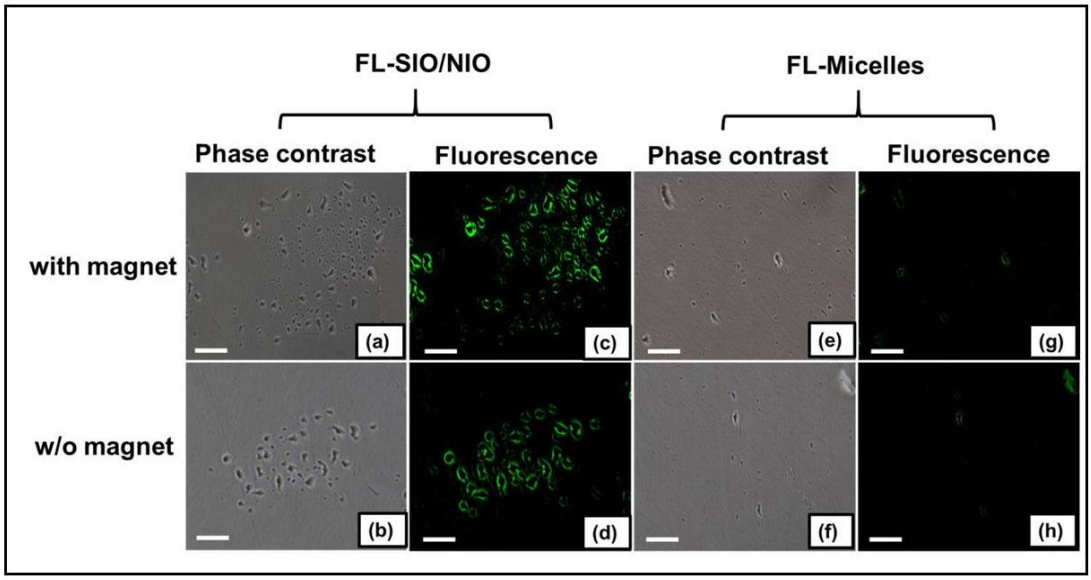

Figure 7:(a,b) and (e,f) are the phase contrast images of FL-SIO/NIO and FL-Micelles respectively with and w/o magnet, (c,d) and (g,h) are the fluorescence microscopic images of FL-SIO/NIO and FL-Micelles respectively again in presence and absence of external magnetic field. Scale bars represent 100µm.

all the treated cells have healthy morphology, indicating the non-toxic nature of both the samples. The corresponding fluorescence microscopic images of the cells (Figure 7: c, d, g, h), obtained using the FITC filter, show robust optical signal from the cytoplasm of cells treated with FL-SIO/NIO magnetosomes, both with and without magnetic guidance (Figure 7: c, d). On the other hand, no discernible fluorescence signal was obtained from cells treated with FL-micelles (Figure 7: g, h). This means that FL entrapped in tween-80 micelles is poorly uptaken by the cells; however, this uptake can be enhanced significantly upon their entrapment within the magnetosomes. It is also worth commenting here that by simple visualization of the cellular fluorescence, it is difficult to state whether magnetic guidance has further enhanced the cellular uptake of FL-entrapped within magnetosomes. We have also observed that cellular entry of nanoparticles is restricted to the cell cytoplasm, and no signal was observed within the nucleus. However, we do not anticipate this to significantly hamper their therapeutic potential as for

successful PDT, nuclear entry is not a strict requirement (unlike in gene therapy where nuclear localization is desired) [37].

Next, the quasi-quantitative analysis of comparative cellular uptake of FL-micelles, and FL entrapped in SIO/NIO magnetosomes, with and without magnetic assistance, was carried out by estimating fluorescence from lysates of treated cells. It can be easily observed (Figure: 8a) that the cellular uptake is higher in case of FL entrapped in magnetosomes, as compared to that of FL-Micelles, thus validating the previous data (Figure 7). Furthermore, for the cells treated with FL-entrapped within magnetosomes, the cellular uptake is enhanced on providing external magnetic assistance, whereas no such enhancement is observed in case of FL-Micelles (p-value<0.05).

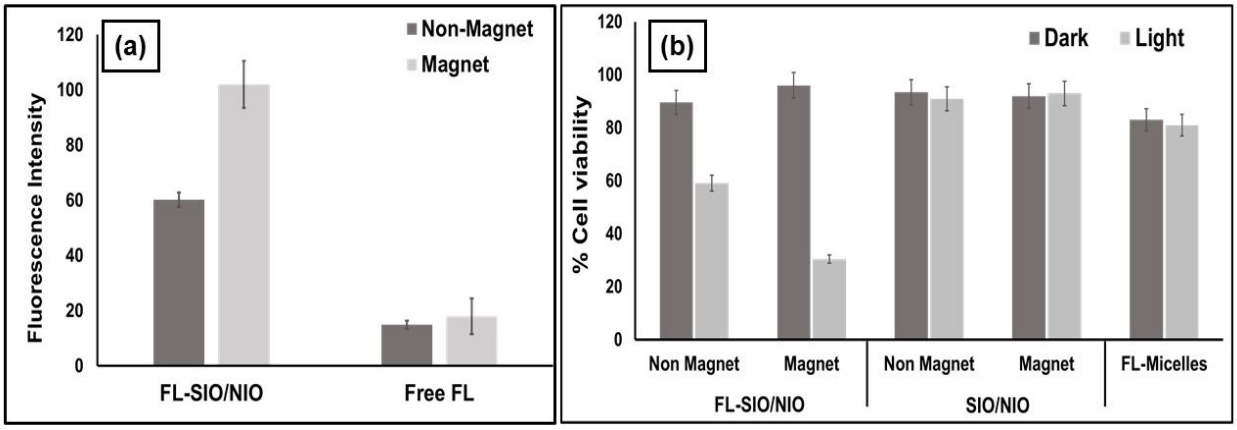

Figure 8:(a) Magnetically induced in vitro cellular uptake of Fluorescein entrapped tween-80(FL-Micelles), fluorescein loaded FL/NIO magnetosomes. (b) Cell viability assay of Panc-1 cells treated with FL-SIO/NIO magnetosomes, placebo SIO/NIO magnetosomes, and FL-micelles, without and with 10 minutes of irradiation with blue light, in presence and absence of the external magnet. The values were found to be statistically significant (p-value<0.05)

Finally, we carried out the photoactivated cell viability assay for FL-Micelles and FL-SIO/NIO magnetosomes, with and without external magnetic assistance. Figure: 8(b) shows that in case of cells treated with FL-Micelles the viability remains around 81% even after the blue light irradiation, while the light induced cytotoxicity was found to be much increased in case of cells

Future Medicine

Version: 19th June 2020

treated with FL-SIO/NIO magnetosomes, showing around 59.2% cell viability. After the use of external magnetic assistance, there is further enhancement in light activated killing of the cancer cells (only 30.5% cells remain viable). Placebo (non FL-loaded) magnetosomes (SIO/NIO) did not show any dark or light-induced toxicity, even after magnetic targeting. Cells treated with FL-Micelles also did not show any substantial dark or light induced toxicity, which can be attributed due to the low cellular uptake of the micelles (p-value<0.05). Hence, these FL-SIO/NIO magnetosomes can be efficiently used in magnetically guided photodynamic therapy for the effective killing of the tumour cells.

Discussion: The efficacy of PDT is limited on a low tissue concentration, mainly explained based on the limitation of photosensitizer penetration in to the target cancer cells. Efficacy can be enhanced by magnetically assisted photodynamic therapy, technique with superior cancer killing properties compared with PDT only. A combination of magnetic and PDT might further improve the $^1O_2$ generation on blue light irradiation. The efficacy of this combined approach has recently been proven where magnetic metal organic framework were used for the magnetically aided delivery of photosensitizer to cancer cells and resulted in the enhanced effect of PDT [38].

In present study, we observed significant decrease in the cancer cells viability (around 30% higher) upon simultaneous light irradiation and application of an external magnetic field. For this purpose, iron oxide nanoparticles were coated with silica shell and entrapped within SIO/NIO along with the FL photosensitizer. We then used this assembly for *in vitro* analysis. The main finding of our study is that around 40% increase in cellular uptake after the effect of magnetic field which in turn increases the $^1O_2$ production over blue light irradiation for the effective killing of cancer cells.

One limitation of FL is that it absorbs only in the low-tissue penetrating blue wavelength region of the visible spectrum, thus making it unsuitable for treating deep-seating lesions using an external light source [37]. However, for treating deeper lesions FL can be easily replaced by other, longer wavelength (e.g. NIR) absorbing photosensitizers within the same 'magnetosome' set-up. Overall, using a proper combination of safe and biocompatible photosensitizers, magnetic nanoparticles and non-ionic surfactants, a photosensitizer-doped magnetosome nanoformulation

Future Medicine
Version: 19th June 2020

can be potentially developed for treating patients with diseases such as cancer and microbial infections in the clinic.

Conclusion:

In this work, silica-coated iron oxide (SIO) nanoparticles and photosensitizer fluorescein (FL) co-entrapped within niosomes, termed as magnetosomes, were prepared. The magnetosomes show efficient loading of the FL and a controlled release of the photosensitizer was observed. *In vitro* studies showed the appreciable cell uptake of the magnetosomes by cancer cells, which is further enhanced by applying the external magnetic assistance because of their superparamagnetic nature. Cell viability assay showed effective killing of cancer cells in the presence of blue light irradiation, which is further enhanced with the help of magnetic targeting. Hence, these magnetosomes have promising applications in magnetically guided photodynamic therapy.

Future Perspective:

The advent of vesicular system represents a significant advancement in the field of magnetically induced photodynamic therapy. The current assembly of these nanoparticles have shown advantages for photodynamic therapy by enhancing the uptake in presence of external magnetic field. The successful applications of magnetically induced PDT *in vitro* confirmed the broad potential of these nanoparticles for future *in vivo* studies. Because of the superparamagnetic behavior, these nanoparticles are excellent candidates as probes for magnetic hyperthermia. The ability to load two different types of drugs at a same time in a single nano-assembly represents an additional value in the design of novel drug delivery platform. It may open new possibilities in the field of nanomedicine and can provide various synergistic effects. Further studies with these nanoparticles should focus on investigating the targeted delivery of nano-assemblies for enhanced efficacy.

Summary Points:

- Double layered niosomes loaded with iron oxide NPs and Fluorescein were synthesized and named as FL loaded magnetosomes.

Future Medicine

Version: 19th June 2020

- FL loaded magnetosomes produce singlet oxygen upon blue light irradiation because of the presence of Fluorescein and showed magnetic properties because of entrapped iron oxide nanoparticles.
- ABMDMA photobleaching assay shows higher singlet oxygen production in FL- loaded magnetosomes in comparison to free FL.
- *In vitro* studies were done using PANC-1 cancer cell lines.
- External magnetic field significantly increases the cellular uptake of the magnetosomes and killing of cancer cells by PDT.
- Fluorescence microscopic images showed enhanced cellular uptake of the magnetosomes aided by external magnetic field.

Figure Legends:

Figure 1: Schematic representation for the synthesis of fluorescein (FL) and SIO nanoparticle co-entrapped niosomes (FL-SIO/NIO).

Figure 2:(a) FTIR spectra of iron oxide (IO), silica coated iron oxide (SIO), and SIO entrapped within niosomes (SIO/NIO), or magnetosomes. (b)Magnetization curve showing superparamagnetic nature of IO and SIO/NIO.

Figure 3: TEM images (a), (b), and DLS graphs (c), (d) of iron oxide (IO) nanoparticles and SIO/NIO magnetosomes.

Figure 4: EDAX spectra of (a) Iron oxide (IO) nanoparticles and (b) SIO/NIO magnetosomes.

Figure 5:(a) UV-Vis spectra of FL-Micelles, (b) Emission spectra of FL-Micelles, FL-SIO/NIO magnetosomes, and SIO/NIO magnetosomes. (c) Percent Release (%) of fluorescein from FL-NIO niosomes, FL-SIO/NIO magnetosomes, and FL-entrapped tween-80 micelles.

Figure 6: A plot between ln (A_t/A_0) versus time(min) by measuring optical density of ABMDMA as a function of time of light irradiation

Future Medicine
Version: 19th June 2020

Figure 7:(a,b) and(e,f) are the phase contrast images of FL-SIO/NIO and FL-Micelles respectively with and w/o magnet, (c,d) and (g,h) are the fluorescence microscopic images of FL-SIO/NIO and FL-Micelles respectively again in presence and absence of external magnetic field. Scale bars represent 100µm.

Figure 8:(a) Magnetically induced in vitro cellular uptake of Fluorescein entrapped tween-80(FL-Micelles), fluorescein loaded FL/NIO magnetosomes. (b) Cell viability assay of Panc-1 cells treated with FL-SIO/NIO magnetosomes, placebo SIO/NIO magnetosomes, and FL-micelles, without and with 10 minutes of irradiation with blue light, in presence and absence of the external magnet. The values were found to be statistically significant (p-value<0.05)

References:

1. Kumar GP, Rajeshwarrao P. Nonionic surfactant vesicular systems for effective drug delivery-an overview. *Acta Pharmaceutica Sinica B.* 1(4), 208-219 (2011).

2. Maibach HI, Choi MJ. Liposomes and Niosomes as topical drug delivery systems. *Skin Pharmacol Physiol.* 18, 209-219 (2005).

‘**’ Comprehensive review about the use of vesicular nanocarriers in drug delivery applications.

3. Sankar V, Ruckmani K, Jailani S et al. Niosome drug delivery system: advances and medical applications an overview. *Pharmacol.* 2, 926-932 (2009).

4. Uchegbu IF, Vyas SP. Non-ionic surfactant based vesicles (niosomes) in drug delivery. *Int J. Pharm.*172(2), 33-70 (1998).

5. Negi LM, Garg AK, Chauhan M. Ultradeformable vesicles: cinceptand execution. *Pharma Times.* 41(9), 11-14 (2009).

6. Lohumi A, Rawat S, Sarkar S et al. A novel drug delivery system: niosomes review. *J. Drug Deliv. Ther.* 2(5), 129-135 (2012).

7. Tu YS, Sun DM, Zhang JJ et al. Preparation and characterisation of andrographolide niosomes and itsanti-hepatocellular carcinoma activity. *J. Microencapsul.* 31(4), 307-16 (2014).

8. De S, Kundu R, Biswas A. Synthesis of gold nanoparticles in niosomes. *J. Colloid Interface Sci.* 386(1), 9 (2012).

‘*’ Example of nanoparticle synthesis and encapsulation within niosomes.

Future Medicine

Version: 19th June 2020

Article Body Template

9. Juneja R, Roy I. Iron oxide-doped niosomes as drug carriers for magnetically targeted drug delivery. *Int. J. Nanomed.* 13, 7-9 (2018).

'*' Example of co-entrapment of iron-oxide nanoparticles and drugs within niosomes.

10. Uchegbu IF, Florence AT. Non-ionic surfactant vesicles (niosomes): Physical and pharmaceutical chemistry. *Adv. Colloid Interface Sci.* 58(1), 1-55 (1995).

1. Bouwstra JA, Van hal DA, Hofland HEJ et al. Preparation and characterization of nonionic surfactant vesicles. *Colloid Surf. A Phy. Eng. Asp.*123-124, 71-80 (1997).

2. Chennam JV, Velchuri S, Chandu BR et al. Niosomes-a novel drug carrier approach. *Int. J. Res Pharm Biomed Sci.* 3(2),722-729 (2012).

3. Cable C. An examination of the effect of surface modifications on the physicochemical and biological properties of non-ionic surfactant vesicles [dissertation]. Glasgow: Univ. of Strathclyde; (1989).

4. Muller JM, Lelievre V, Giraudon LB et al. VIP as a cell-growth and differentiation neuromodulator role in neurodevelopment. *Mol. Neurobiol.* 10(2-3), 115-34 (1995).

5. Beloshe P, Jadhav R, Zorn S et al. Niosomes: as novel drug delivery system. *Int. J. Pharm. Pharm. Sci.* 4(2), 73-78 (2019).

6. Abdelbary A, Salem HF, Khallaf RA. Niosomal 5-Flourouracil gel for effective treatment of skin cancer; In-vitro and In-vivo evaluation. *Int. J. Drug Deliv.* 7(4), 223-232 (2016).

7. Sheenal IP, Singh UV, Kamath R et al. Niosomal withaferin A with better antitumor efficacy. *Int. J. Pharm. Sci.* 60(1), 45-48 (1998).

8. Solanki AB, Parikh JR, Parikh RH et al. Evaluation of different compositions of niosomes to optimize aceclofenac transdermal delivery. *Asian J. Pharm. Sci.* 5(3), 87-95 (2010).

9. Kubler AC, Haase T, Staff C et al. Photodynamic therapy of primary nonmelanomatous skin tumours of the head and neck. *Laser Surg. Med.* 25(1), 60-8 (1999).

'*' Example of treatment of cancer using photodynamic therapy.

20. D. -C. Nina, S. Grafe, B. Gitter et al. Surface charged temporfin-loadedflexible vesicles: in vitro skin penetration studies and stability. *Int. J. Pharm.* 384(1-2), 100-8 (2010).

21. Abed Z, Beik J, Laurent S et al. Iron-oxide-gold core-shell nano-theranostic for magnetically targeted photothermal therapy under magnetic resonance imaging guidance. *J Canc Res Clin Oncol,* 145, 1213-1219 (2019).

'*' Example of magnetic targeting of iron oxide-based nanoparticles and further application in MRI-guided photothermal therapy

22. T. Kubo, T. Sugita, S. Shimose et al. Targeted delivery of anticancer drugs with intravenously administered magnetic liposomes in osteosarcoma-bearing hamsters. *Int. J. Oncol.* 17(2), 309-15 (2000).

23. X. Battle, A. Labarta. Finite-size effects in fine particles: magnetic and transport properties. *J. Phys. D: Appl. Phys.* 35, R15-R42 (2002).

24. Zheng H, Li J, Wang ZL et al. Bimagnetic Core/Shell FePt/Fe3O4 nanoparticles. *Nano Lett.* 4(1),187-190 (2004).

25. Frenkel J, Dorfman J. Spontaneous and induced magnetisation in ferromagnetic bodies. *Nature.* 126, 274-275 (1930).

26. Vazquez M, Luna C, Morales MP et al. Magnetic nanoparticles: synthesis, ordering and properties. *Phys. B: Condensed Matter.* 354(1-4), 71-79 (2004).

'**' Excellent review on the preparation of magnetic nanoparticles with desired magnetic properties.

27.Beik J, Asadi M, Khoei S et al. Simmulation-guided photothermal therapy using MRI-traceable iron oxide nanoparticles. *J. Photochem. Photobiol. B, Biol.* 199, 111599 (2019).

28. Shirvalilou S, Khoei S, Khoee S et al. Development of a magnetic nano-graphene oxide carrier for improved glioma targeted drug delivery and imaging: in vitro and in vivo evaluations. *Chem. Biol. Interact*, 295, 97-108 (2018).

29. Hosseini V, Mirrahimi M, Zadeh A et al. Multimodal cancer cell therapy using Au@Fe_2O_3 core-shell nanoparticles in combination with photo-thermo-radiotherapy, *Photodiagnosis photodyn Ther.* 24, 129-135 (2018).

30. Montazerabadi A, Beik J, Irajirad R et al. Folate-modified and curcumin-loaded dendritic magnetite nanocarriers for the targeted thermo-chemotherapy of cancer cells, *Artif Cells Nanomed Biotechnol.* 47(1), 330-340 (2019).

Future Medicine

Version: 19th June 2020

31. Kim S, Fujitsuka M, Majima T. Photochemistry of singlet oxygen sensor green. *J. Phys. Chem. B.* 45, 13985-13992 (2013).

32. Tanaka K, Miura T, Umezawa N et al. Rational design of fluorescein-based fluorescence probes. Mechanism-based design of a maximum fluorescence probe for singlet oxygen. *J. Am. Chem. Soc.* 123, 2530-2536 (2001).

33. Shibu ES, Sugino S, Ono K et al. Singlet-oxygen-sensitizing near-infrared-fluorescent multimodal nanoparticles. *Angew Chem. Int. Ed.* 52(40), 10559-63 (2013).

'*' Example of nanoparticle-mediated production of light-activated singlet oxygen.

34. Kaushik A, Khan R, Solanki PR et al. Iron oxide nanoparticles-chitosan composite based glucose biosensor. *Biosens. Bioelectron.* 24(4), 676-83 (2008).

35. Akbarzadeh, Zarghami N, Mikaeili H et al. Synthesis, characterization, and in vitro evaluation of novel polymer-coated magnetic nanoparticles for controlled delivery of doxorubicin. *Nanotechnology, Science and Applications.* 5, 13-25 (2012).

36. Kodama RH. Magnetic nanoparticles. *J. Magn. Magn. Mater.* 200(1-3), 359-372 (1999).

37. Chen G, Roy I, Yang C, Prasad PN. Nanochemistry and Nanomedicine for Nanoparticle-based Diagnostics and Therapy. *Chem. Rev.* 116(5), 2826-85 (2016)

'**' Comprehensive review about the use of nanoparticles in biomedical applications

38. Sharma S, Sethi K, Roy I. magnetic nanoscale metal-organic frameworks for magnetically aided drug delivery and photodynamic therapy. *New J. Chem.* 41,11860-11866 (2017).